

Contact-FP: A Dimerization-Dependent Fluorescent Protein Toolkit for Visualizing Membrane Contact Site Dynamics

Contact
Volume 7: 1–12
© The Author(s) 2024
Article reuse guidelines:
sagepub.com/journals-permissions
DOI: 10.1177/25152564241228911
journals.sagepub.com/home/ctc



Gregory E. Miner , Sidney Y. Smith, Wendy K. Showalter, Christina M. So, Joey V. Ragusa, Alex E. Powers, Maria Clara Zanellati , Chih-Hsuan Hsu, Michelle F. Marchan, and Sarah Cohen 

Abstract

Membrane contact sites (MCSs) are sites of close apposition between two organelles used to exchange ions, lipids, and information. Cells respond to changing environmental or developmental conditions by modulating the number, extent, or duration of MCSs. Because of their small size and dynamic nature, tools to study the dynamics of MCSs in live cells have been limited. Dimerization-dependent fluorescent proteins (ddFPs) targeted to organelle membranes are an ideal tool for studying MCS dynamics because they reversibly interact to fluoresce specifically at the interface between two organelles. Here, we build on previous work using ddFPs as sensors to visualize the morphology and dynamics of MCSs. We engineered a suite of ddFPs called Contact-FP that targets ddFP monomers to lipid droplets (LDs), the endoplasmic reticulum (ER), mitochondria, peroxisomes, lysosomes, plasma membrane, caveolae, and the cytoplasm. We show that these probes correctly localize to their target organelles. Using LDs as a test case, we demonstrate that Contact-FP pairs specifically localize to the interface between two target organelles. Titration of LD-mitochondria ddFPs revealed that these sensors can be used at high concentrations to drive MCSs or can be titrated down to minimally perturb and visualize endogenous MCSs. We show that Contact-FP probes can be used to: (1) visualize LD-mitochondria MCS dynamics, (2) observe changes in LD-mitochondria MCS dynamics upon overexpression of PLIN5, a known LD-mitochondrial tether, and (3) visualize two MCSs that share one organelle simultaneously (e.g., LD-mitochondria and LD-ER MCSs). Contact-FP probes can be optimized to visualize MCSs between any pair of organelles represented in the toolkit.

Keywords

membrane contact sites, fluorescent proteins, biosensors, organelles, lipid droplets, endoplasmic reticulum, mitochondria, peroxisomes, lysosomes, plasma membrane, caveolae

Introduction

Eukaryotic cells are compartmentalized into membrane-bound organelles, allowing for the spatial separation of incompatible biochemical processes. Nevertheless, organelles must communicate for the cell to function as an integrated unit. One way that organelles communicate is at membrane contact sites (MCSs), sites of close apposition between the membranes of two organelles (Scorrano et al., 2019). Recent work has highlighted an increasing list of functions for MCSs, including roles in the exchange of ions, lipids, and proteins, as well as in organelle biogenesis and division (Prinz et al., 2019). Cells can modulate MCSs to adjust their metabolism in response to changing environmental or developmental conditions (Bohnert, 2020). Thus, there is a need for methods to visualize MCSs accurately and precisely in live cells. This has been challenging due to the small size and dynamic nature of these structures. Electron microscopy is considered the gold standard for

identifying MCSs but is incompatible with live-cell imaging. Diffraction-limited fluorescence microscopy of cells expressing organelle markers can be used to measure organelle proximity and to infer changes in MCSs in response to different conditions (Valm et al., 2017). However, because MCSs are defined as occurring between membranes that are within a 30 nm distance (Scorrano et al., 2019), diffraction-limited microscopy cannot

Department of Cell Biology and Physiology, University of North Carolina at Chapel Hill, Chapel Hill, North Carolina, USA

Received September 28, 2023; Accepted January 11, 2024

Corresponding Author:

Sarah Cohen, Department of Cell Biology and Physiology, University of North Carolina at Chapel Hill, Chapel Hill, North Carolina, 27599, USA.
Email: sarahcoh@med.unc.edu



distinguish whether two organelles are in close proximity or truly form a *bone-fide* MCS.

A variety of probes to detect MCSs have been developed to overcome these challenges. Bimolecular fluorescence complementation systems have been used to study multiple different MCSs (Jing et al., 2020). These systems involve targeting nonfluorescent fragments of fluorescent proteins (FPs) to two different organelles; when the organelles come together, the fluorophore is reconstituted, fluorescing only at the interface between the two membranes. Split green fluorescent protein (GFP)-based contact site sensors have been developed for endoplasmic reticulum (ER)-mitochondria, ER-plasma membrane, ER-peroxisome, and mitochondria-peroxisome MCSs in mammalian cells (Cieri et al., 2017; Vallese et al., 2020). In *Saccharomyces cerevisiae*, split GFP- or split Venus-based probes have been used to investigate MCSs between nearly every pair of membrane-bound organelle (Kakimoto et al., 2018; Shai et al., 2018). These bimolecular fluorescence complementation systems are useful for detecting differences in the number and extent of MCSs under various conditions, and in screens to identify new tethers at MCSs (Lahiri et al., 2014; Shai et al., 2018; Yang et al., 2018; Castro et al., 2022). However, because the fluorescence complementation of split FPs is irreversible, these probes tend to stabilize MCSs and are therefore not ideal for studying MCS dynamics.

Dimerization-dependent FPs (ddFPs) have emerged as an alternative tool for studying MCSs. ddFPs consist of a weakly fluorescent monomeric protein and a nonfluorescent monomeric protein that reversibly interact to form a fluorescent heterodimeric complex. The original ddFP was based on red FP and was initially used to detect protein-protein interactions and caspase activity (Alford et al., 2012a). An extended palette in which green A (GA) or red A (RA) monomers can be complemented interchangeably with a B monomer was subsequently developed (Ding et al., 2015). Although ddFPs have primarily been used to study protein-protein interactions, the ddFP system has been adapted to detect MCSs including ER-mitochondria (Alford et al., 2012b; Naon et al., 2016; Nguyen and Voeltz, 2022), ER-P-body (Lee et al., 2020), or mitochondria-mitochondria (Abrisch et al., 2020) contacts. Because the interaction between ddFP monomers is reversible, ddFPs are more amenable than split FP systems for studying MCS dynamics. The main disadvantage of ddFPs is their lower fluorescence relative to split FPs. However, we have found that with the availability of increasingly sensitive microscope detectors, this disadvantage can now be overcome.

Here, we build on previous work using ddFPs to visualize the morphology and dynamics of MCSs. We engineered a suite of ddFPs called Contact-FP that targets the three ddFP monomers (RA, GA, and B) to eight subcellular compartments: lipid droplets (LDs), ER, mitochondria, peroxisomes, lysosomes, plasma membrane, caveolae, and the cytoplasm. Using complementary cytoplasmic monomers (GA or B), we show that the seven organelle probes correctly localize to their targets. We demonstrate that Contact-FP pairs specifically localize to the

interface between target organelles for each LD-organelle pair. We found that by titrating LD-mitochondria ddFPs, we could either induce MCSs at high concentrations or minimally perturb and visualize endogenous MCSs at lower concentrations. Finally, we demonstrate several use cases for LD-mitochondria and LD-ER ddFPs. Theoretically, Contact-FP probes can be optimized to visualize MCSs between any pair of organelles represented in the toolkit, although several optimization steps are required for each new ddFP pair.

Results

Design of Contact-FP Probes

Recent studies have demonstrated the use of ddFPs to visualize MCS dynamics (Alford et al., 2012b; Naon et al., 2016; Abrisch et al., 2020; Lee et al., 2020; Nguyen and Voeltz, 2022). Due to relatively low heterodimer affinity, the binding of ddFPs is reversible and therefore can be used to visualize MCS dynamics without artificially stabilizing them (Figure 1A). While ddFPs represent a promising tool for the study of MCS, constructs have only been made to target a small subset of organelle membranes. To expand the use of ddFPs for studying MCSs, we generated a ddFP construct library targeting ddFP monomers (GA, RA, and B) to the cytoplasm or the cytoplasmic-facing membrane of seven organelles including the LD, ER, mitochondria, peroxisomes, lysosomes, plasma membrane, and caveolae. We named this suite of probes Contact-FP, analogous to Contact-ID, a split-pair BioID for identifying proteins at MCSs by proteomics (Kwak et al., 2020). Minimal membrane targeting domains were used to localize ddFPs when possible, to minimize disruption of organelle function (Figure 1B). To target ddFP monomers to the LD or peroxisome membrane we used the hairpin domain of GPAT4 (Wang et al., 2016; Chang et al., 2019) or the membrane targeting sequence of PEX3 (Soukupova et al., 1999) respectively, which we have successfully used previously to localize chimeric proteins (Miner et al., 2023). Monomers were targeted to the ER and mitochondrial membranes using the transmembrane domains of CYP2C1 and MAVS, respectively (Cho et al., 2020). Plasma membrane-targeted monomers were localized using the palmitoylation domain of GAP43 (Chung et al., 2019). Finally, due to a lack of well-established specific targeting domains, ddFP monomers were targeted to lysosomes and caveolae by fusing with lysosomal-associated membrane protein 1 (LAMP1) or caveolae-associated protein 1 (CAVIN1), respectively.

Contact-FP Probes Localize to Their Target Organelles

We next tested whether our organelle-targeted monomers properly localized to the cytoplasmic face of the intended organelle membrane by coexpressing them with the cytoplasmic heterodimeric partner (Figure 2A). For these experiments, we used the GA monomer constructs as these exhibit higher brightness and contrast than the RA monomer

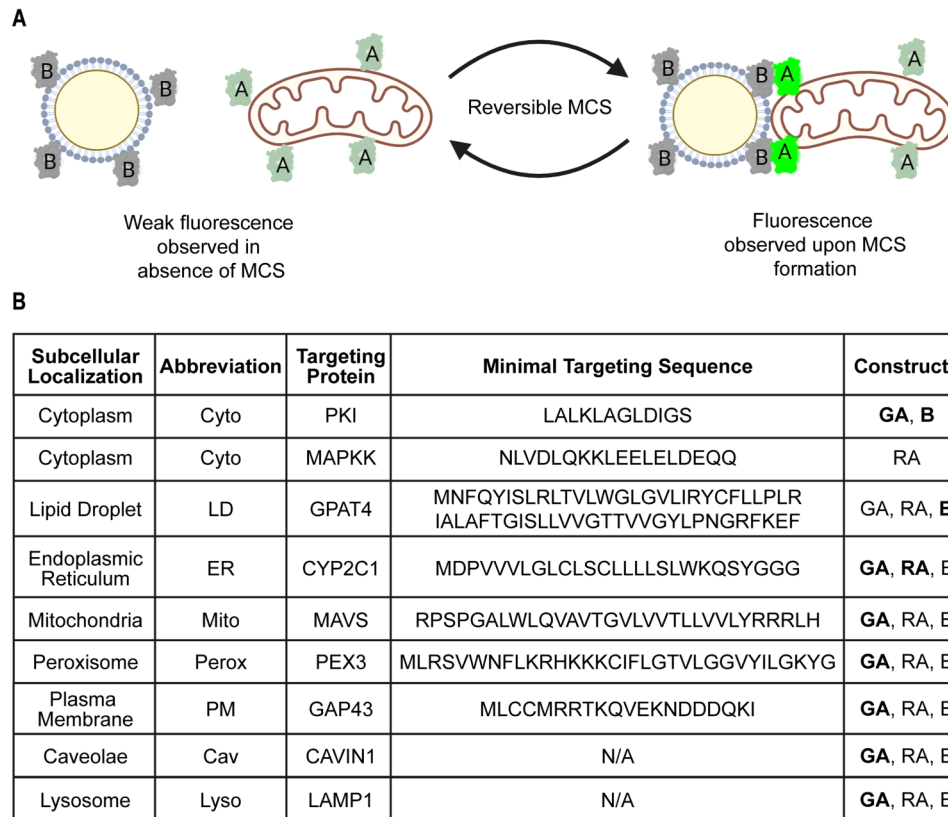


Figure 1. Design of Contact-fluorescent protein (Contact-FP) probes. (A) Cartoon of reversible Contact-FP probe system. Monomers targeted to distinct cellular membranes reversibly dimerize when in close proximity (~10–30 nm) resulting in increased fluorescence of the “A” monomer at membrane contact sites. Cartoon created with Biorender.com. (B) List of probes generated for the Contact-FP library. The targeting sequence used to localize probes and the source protein are included. The probes demonstrated within this study are bolded.

probes, and therefore were ideal for initial optimization and evaluation of novel ddFP constructs. We found that the coexpression of cytoplasmic monomer with our organelle-anchored monomers resulted in a fluorescence signal along the entire surface of the organelle of interest (Figure 2B–H). Localization was confirmed by comparing localization with known fluorescent organelle markers by confocal microscopy. Given that ER proteins can be restricted to either ER tubules or sheets, we utilized Airyscan superresolution imaging to resolve both substructures and confirmed localization of ER-tethered GA along the entire ER surface. While most constructs labeled the target organelle following a 24-h transfection, LD-targeted constructs required 48 h for efficient labeling of LDs. Unlabeled LDs likely represent mature LDs detached from the ER which cannot be labeled by membrane-anchored proteins that require ER-LD bridges for trafficking (Wilfling et al., 2013).

LD-Organelle Contact-FP Pairs Correctly Localize to MCSs

Having confirmed that the Contact-FP constructs properly localize, we next validated their use to specifically detect

MCSs. For these experiments, we focused on studying LD-organelle MCSs. LDs are an ideal use of Contact-FP as they form dynamic and transient MCSs with all organelles included in our set of constructs (Valm et al., 2017; Matthaeus and Taraska, 2021). Specifically, we tested whether organelle-tethered GA monomers would brightly fluoresce when colocalized with an LD-tethered B monomer (LD-B) at LD-organelle MCSs (Figure 3A). As expected, we were able to observe LD-organelle contacts with all organelles tested and found that GA fluorescence was brightest at sites of organelle marker colocalization (Figure 3B–G). It was necessary to optimize the ratio of GA and B probes for each pair of organelles. Factors that could affect the amount of probe needed include the specific turnover rate of each probe and the abundance of the MCS being studied.

The abundance of MCSs varied greatly depending on the LD-organelle pair. For example, most LDs in cells transfected with mitochondria-targeted GA (Mito-GA) and LD-B were positive for GA signal (Figure 3B), indicating that LD-mitochondria contacts are abundant in U-2 OS cells. In contrast, the GA signal was only observed on LDs at the cell periphery in cells expressing plasma membrane-targeted

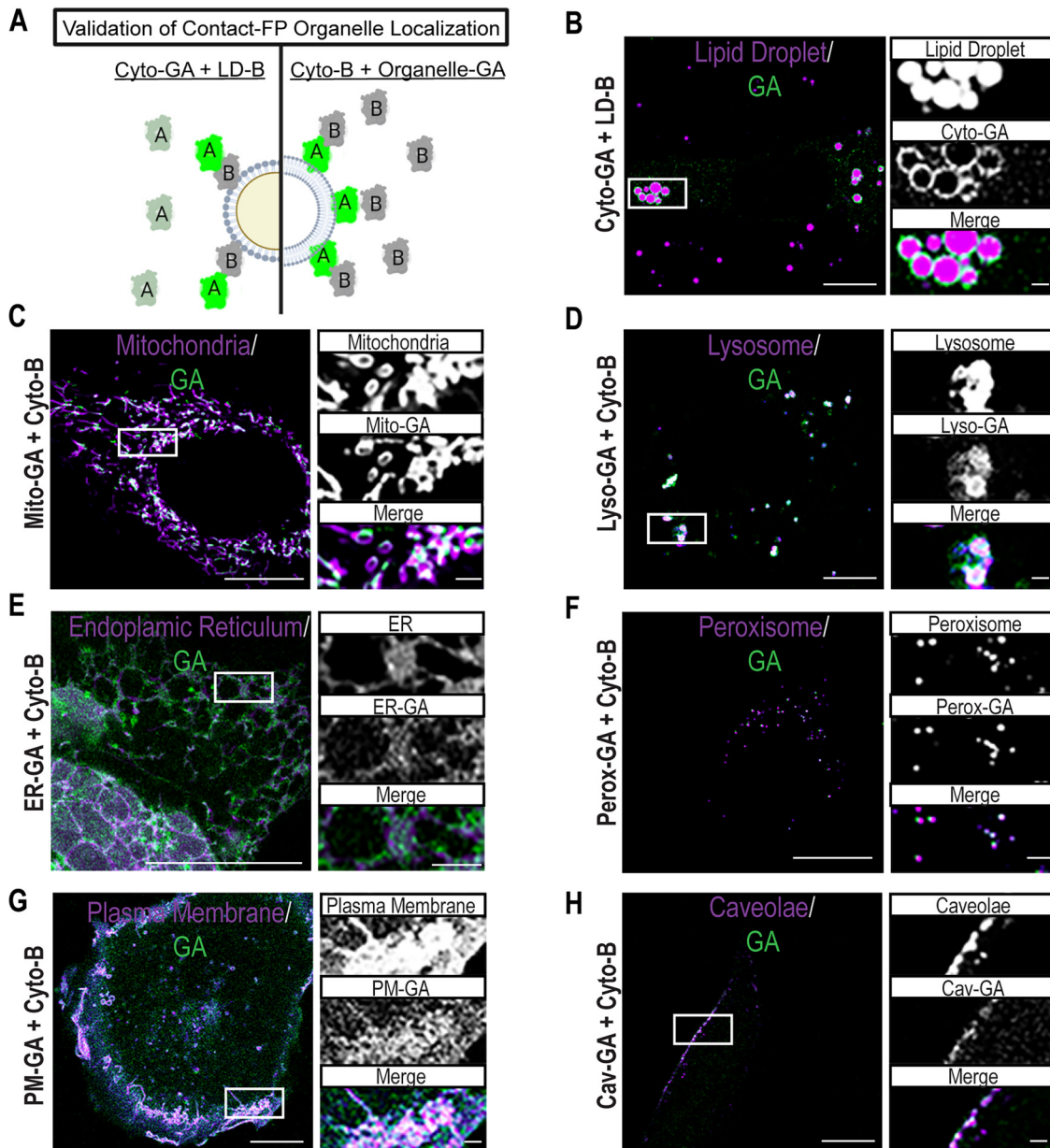


Figure 2. Contact-FP probes localize to their target organelles. (A) Cartoon depicting the use of cytoplasmic Contact-FP probes (Cyto-GA and Cyto-B) to validate cellular localization of organelle membrane-targeted probes. Cartoon created with Biorender.com. (B) Single focal plane micrographs of U-2 OS cells transfected with the indicated Contact-FP probes and labeled for LDs with Bodipy 665/676. Merged micrograph includes GA and Bodipy 665/667 channels to demonstrate colocalization (white). (C–H) Single focal plane micrographs of U-2 OS cells transfected with the indicated Contact-FP probes and labeled for organelles with (C) mApple-TOMM20-N-10, (D) mApple-Lysosomes-20, (E) mApple-Sec61B, (F) mApple-Peroxisomes-2, (G) mApple-Farnesyl-5, and (H) mApple-Caveolin-C-10. Merged micrograph includes GA and mApple channels to demonstrate colocalization (white).

(C, E, F) U-2 OS cells were imaged using Airyscan.

Scale bar, 10 μ m. Inset scale bar, 1 μ m.

Note. Contact-FP = Contact-fluorescent protein; LD = lipid droplet; GA = green A.

GA and LD-B (Figure 3F), indicating that only a subset of LDs form MCSs with the plasma membrane in U-2 OS cells. Qualitatively, organelle morphology did not appear disrupted by the expression of ddFP probes. The exception was that upon expression of peroxisome-targeted GA (Pero-GA)

and LD-B, rings of peroxisomes were observed around LDs in cells with detectable GA signal (Figure 3E), while the GA signal was not detectable in the majority of transfected cells. Rings of peroxisomes were never observed in control cells. We interpret this to mean that LD-peroxisome contacts are

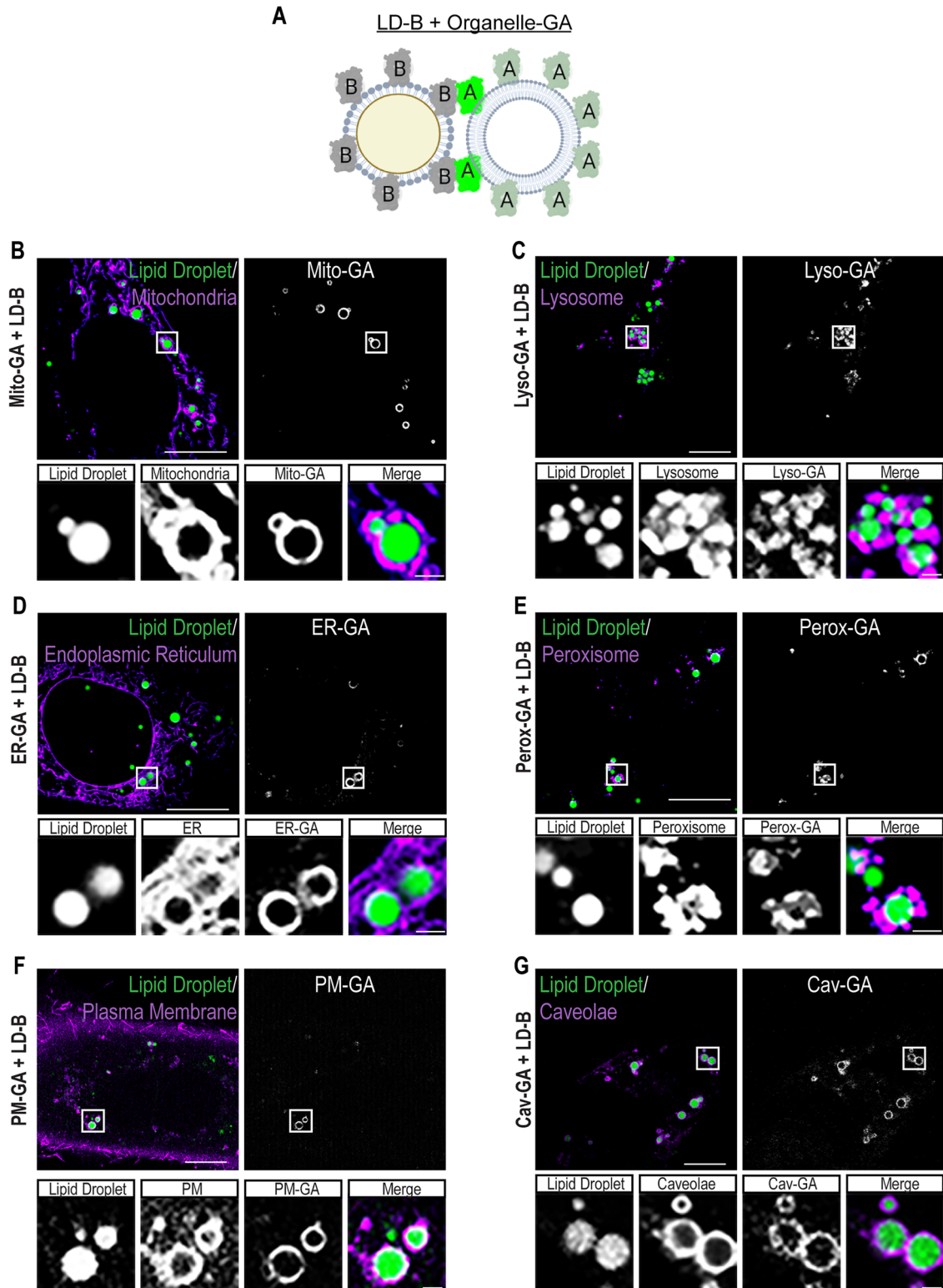


Figure 3. LD-organelle Contact-FP pairs correctly localize to MCSs. (A) Cartoon depicting the use of Contact-FP probes (organelle-GA and LD-B) to validate Contact-FP fluorescence at MCSs. Cartoon created with Biorender.com. (B–G) Single focal plane micrographs of U-2 OS cells transfected with the indicated Contact-FP probes, labeled for LDs with Bodipy 665/676, and labeled for organelles with (B) mApple-TOMM20-N-10, (C) mApple-Lysosomes-20, (D) mApple-Sec61B, (E) mApple-Peroxisomes-2, (F) mApple-Farnesyl-5, and (G) mApple-Caveolin-C-10. Merged micrographs include Bodipy 665/676 and mApple channels (but not GA) to demonstrate LD-organelle MCSs (white). (B, D, E) U-2 OS cells were imaged using Airyscan. Scale bar, 10 μm. Inset scale bar, 1 μm. Note. LD = lipid droplet; Contact-FP = Contact fluorescent protein; MCS = membrane contact site; GA = green A; LD-B = LD-tethered B monomer.

rare in U-2 OS cells. Thus, the only cells in which we detected GA signal were those in which ddFPs were expressed at concentrations high enough to induce the formation of MCSs.

LD-Mitochondria Contact-FP Probes can be Titrated to Induce or Visualize MCSs

Given the low affinity of the heterodimeric monomers and therefore reversible binding, we hypothesized that induced MCS formation (e.g., in the case of LD-peroxisome MCSs) was a consequence of high Contact-FP expression. A major goal of our Contact-FP probes is the ability to monitor MCS dynamics while not perturbing MCS formation. Therefore, we tested whether the expression of Contact-FP pairs could be titrated to avoid MCS induction while retaining a robust signal. We expressed varying amounts of Mito-GA together with a constant level of LD-B (Figure 4). We found that expressing high concentrations of Mito-GA caused a significant increase in LD-mitochondria colocalization and a corresponding increase in GA fluorescence at LDs relative to controls expressing only a single monomer (Figure 4A, B, E, and F). In contrast, reduced expression of Mito-GA did not significantly induce LD-mitochondria contacts, while a strong GA signal was retained at contact sites (Figure 4C, E, and F and Supplemental Figure S1A–C). Further reduction of Mito-GA expression resulted in a visible yet faint GA signal at the LD-mitochondria MCS (Figure 4D–F). Taken together, we demonstrate that the expression of Contact-FP probes can be used to either induce MCSs at high concentrations or to visualize MCS dynamics without artificial contact site induction at low concentrations.

Use Cases for Contact-FP Probes: LD-Mitochondria Dynamics in Response to Overexpression of Known Tethers and Visualizing Multiple MCSs

Our data thus far demonstrate that Contact-FP probes properly localize to their target organelle membranes and can be used to visualize MCSs without MCS induction. Finally, we wanted to demonstrate the potential uses of our Contact-FP probes. We first tested the use of our LD-mitochondria Contact-FP probes to investigate the effect of PLIN5 overexpression on LD-mitochondria MCS dynamics (Figure 5). PLIN5 is a well-established LD-mitochondria tether that has been shown to induce membrane contacts upon overexpression and reduce LD mobility (Wang et al., 2011; Miner et al., 2023). As anticipated, we observed a drastic increase in LD-mitochondria contacts following overexpression of PLIN5 and an increase in GA fluorescence relative to controls (Figure 5A, B, E, F, and G). Intriguingly, time-lapse imaging showed that LD-mitochondria MCSs in control cells are highly dynamic and typically only cover a portion of the LD surface. Over time we observed rapid changes in MCS area at individual LDs, with

LD-mitochondria contact sites growing and shrinking (Figure 5C and Supplemental Figure S2A). In contrast, LDs in cells expressing PLIN5 appear enveloped by mitochondria with extensive LD-mitochondria MCSs. Additionally, these MCSs appear extremely stable and no longer change in size over time (Figure 5D). This example illustrates the ability to use Contact-FP to directly visualize MCS dynamics.

Another advantage of Contact-FP is the ability to choose from constructs containing a fluorescent GA or RA monomer, which fluoresce at green and red wavelengths, respectively. Since both GA and RA monomers can form heterodimeric pairs with the B monomer, this opens the possibility to monitor two MCSs simultaneously. As the LD is known to interact extensively with both mitochondria and the ER, we assessed whether we could visualize both LD-mitochondria and LD-ER MCSs in the same cell (Figure 6A). We found that the coexpression of Mito-GA and ER-RA with LD-B allowed simultaneous visualization of both LD-mitochondria and LD-ER MCSs (Figure 6B and C). As expected, GA and RA signal colocalize with LDs (Figure 6B) and respective organelle membranes (Figure 6C). Furthermore, RA and GA signals are spatially distinct with no significant crosstalk. Intriguingly, while most LDs appear to form MCSs with either mitochondria or ER, we also observed cases where a single LD forms three-way MCSs with both mitochondria and ER (Figure 6C, inset). While LDs that formed dual contacts with the mitochondria and ER represented a small fraction of all LDs (~8%), these may be highly active sites of metabolism and will be of interest in future investigations (Figure 6D).

Discussion

Here, we have built on previous work using ddFPs as sensors to visualize MCSs. We engineered a suite of ddFPs called Contact-FP that targets ddFP monomers to seven organelles or the cytoplasm. We show that these probes correctly localize to their target organelles and that Contact-FP pairs specifically localize to the interface between target organelles. Contact-FP can be used at high concentrations to drive MCSs or can be titrated down to minimally perturb and visualize endogenous MCSs. We demonstrated several use cases for Contact-FP probes, including the observation of changes in LD-mitochondria MCS dynamics upon overexpression of PLIN5, and the visualization of two MCSs that share one organelle simultaneously.

Contact-FP probes can be used to visualize MCSs between any pair of organelles represented in the toolkit. However, optimization is required for each organelle pair and is cell-type dependent. For example, when expressed at high concentrations we found that coexpression of Perox-GA and LD-B-induced peroxisome-LD contacts in U-2 OS cells and resulted in elongated contact sites. The elongation of these contact sites, in contrast to the expected point contacts between two spheres, suggests that deformation of one or both organelles is occurring.

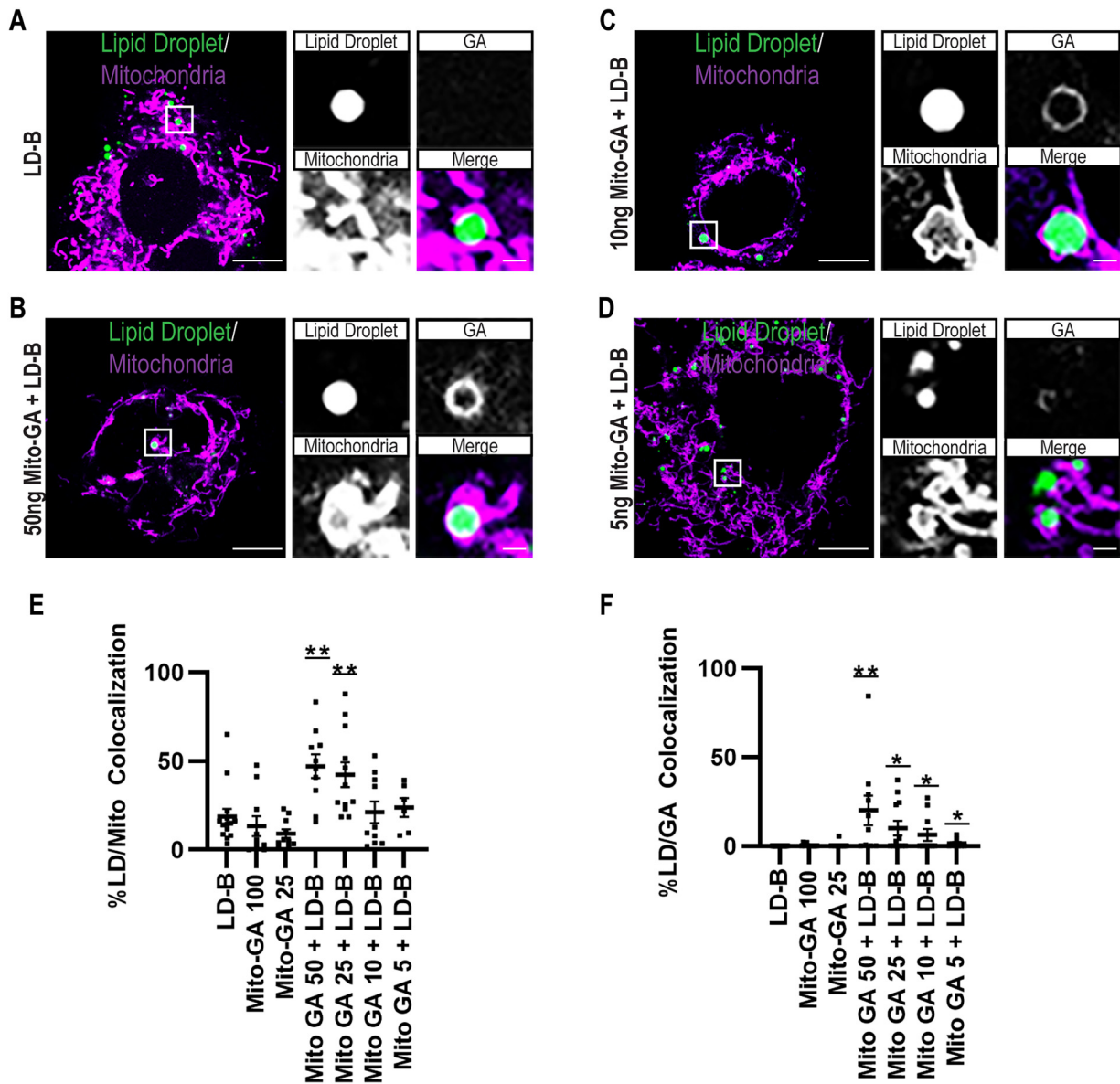


Figure 4. LD-mitochondria Contact-FP probes can be titrated to induce or visualize MCSs. (A–D) Single focal plane micrographs of U-2 OS cells transfected with the indicated Contact-FP probes, labeled for LDs with Bodipy 665/676, and labeled for mitochondria with mApple-TOMM20-N-10. Merged micrograph includes Bodipy 665/676 and mApple channels (but not GA) to demonstrate LD-organelle MCSs (white). (E, F) Quantification of images from (A–D). (E) Colocalization of LDs with mitochondria was measured as % LD pixels overlapping with mitochondria, and (F) Colocalization of LDs with Mito-GA was measured as % LD pixels overlapping with Mito-GA. At least ten cells were analyzed across $N = 3$ biological replicates for all conditions except for 5 ng Mito-GA + LD-B which had six cells analyzed. Scale bar, 10 μm . Inset scale bar, 1 μm . Error bars represent \pm SEM. * $p < .05$, ** $p < .01$.
 Note. LD = lipid droplet; Contact-FP = contact-fluorescent protein; MCS = membrane contact site; GA = green A; LD-B = LD-tethered B monomer; Mito-GA = mitochondria-targeted green A; SEM = standard error of the mean.

To investigate MCS dynamics, we recommend performing titration experiments such as in Figure 4 to determine the minimal expression of a Contact-FP pair that provides a robust signal without inducing MCSs or disrupting organelle morphology in a given cell type. Making stable cell lines or introducing ddFPs via CRISPR may provide the most consistent cell-to-cell expression levels of ddFPs. The main advantage of ddFPs over bimolecular fluorescence complementation

systems such as split GFP is that ddFP dimerization is reversible, allowing the visualization of MCS dynamics with minimal perturbation of the endogenous MCS. However, the disadvantage is that ddFPs are not as bright as split FPs. For most of the LD-organelle MCSs we imaged, we found that confocal microscopy was sufficiently sensitive to detect GA signals at contact sites. However, several MCSs benefitted from more sensitive methods such as Airyscan microscopy.

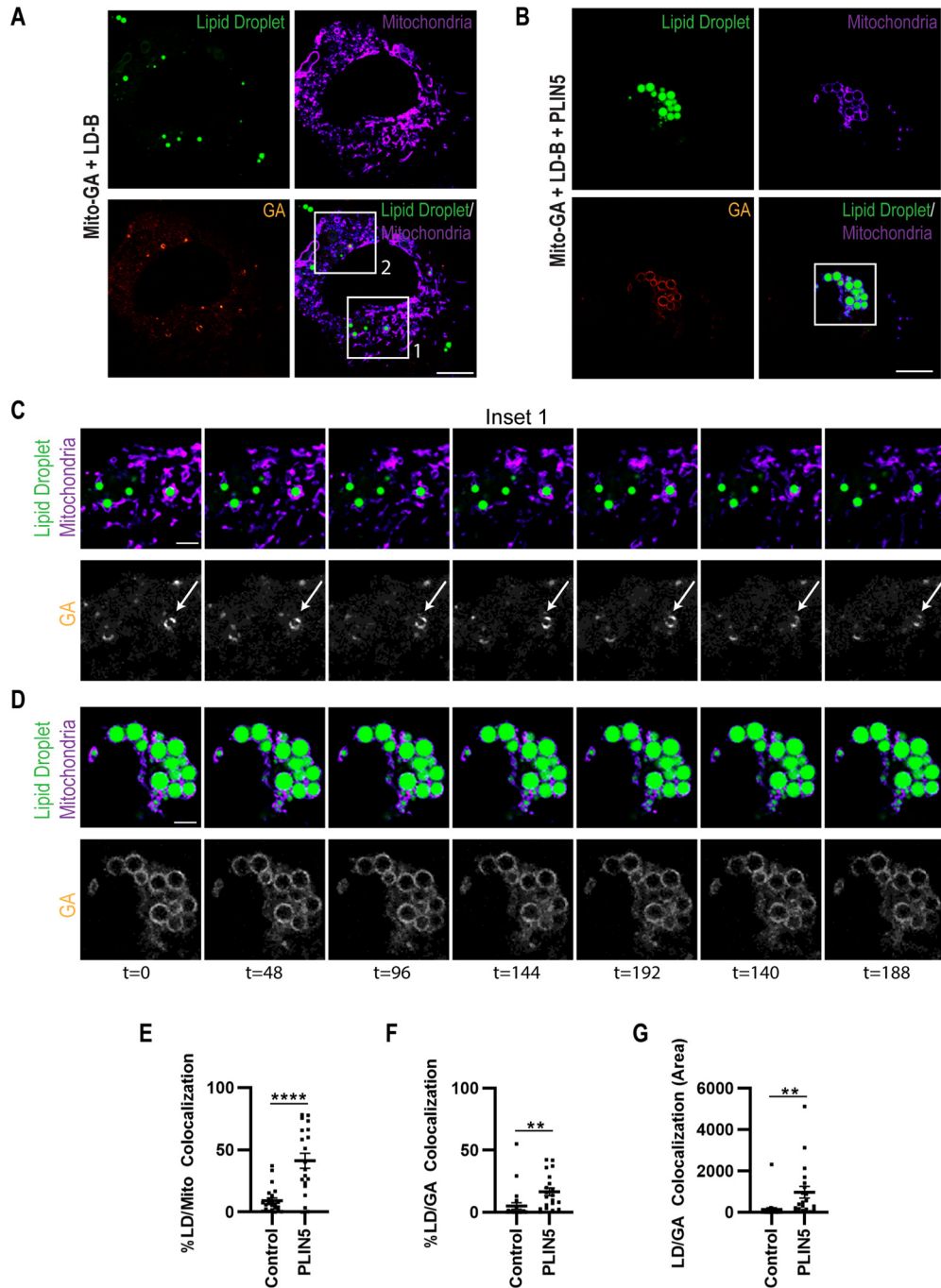


Figure 5. Use case for Contact-FP probes: LD-mitochondria dynamics in response to overexpression of a known tether. (A, B) Single focal plane micrographs of U-2 OS cells transfected with the indicated constructs, labeled for LDs with Bodipy 665/676, and labeled for mitochondria with mApple-TOMM20-N-10. Merged micrograph includes Bodipy 665/676 and mApple channels to demonstrate LD-organelle MCSs (white). (C) Inset 1 (from panel A) shows dynamics of LD-mitochondria MCSs over a 3 min time-lapse movie with frames captured every 12 s. The white arrow indicates an LD-mitochondria MCS that dissipates during the movie. (D) Inset (from panel B) shows decreased dynamics of LD-mitochondria MCSs in cells overexpressing the LD-mitochondria tether PLIN5 over a 3 min time-lapse movie with frames captured every 12 s. Scale bar, 10 μ m. Inset scale bar, 2 μ m. (E–G) Quantification of images from (A, B). (E) Colocalization of LDs with mitochondria was measured as % LD pixels overlapping with mitochondria, (F) colocalization of LDs with Mito-GA was measured as % LD pixels overlapping with Mito-GA, (G) area of LD colocalization with Mito-GA was measured as total LD pixels overlapping with Mito-GA. At least 20 cells were analyzed across $N = 3$ biological replicates for all conditions. Error bars represent \pm SEM. ** $p < .01$, **** $p < .0001$.

Note. Contact-FP = contact-fluorescent protein; LD = lipid droplet; MCS = membrane contact site; GA = green A; SEM = standard error of the mean; Mito-GA = mitochondria-targeted green A.

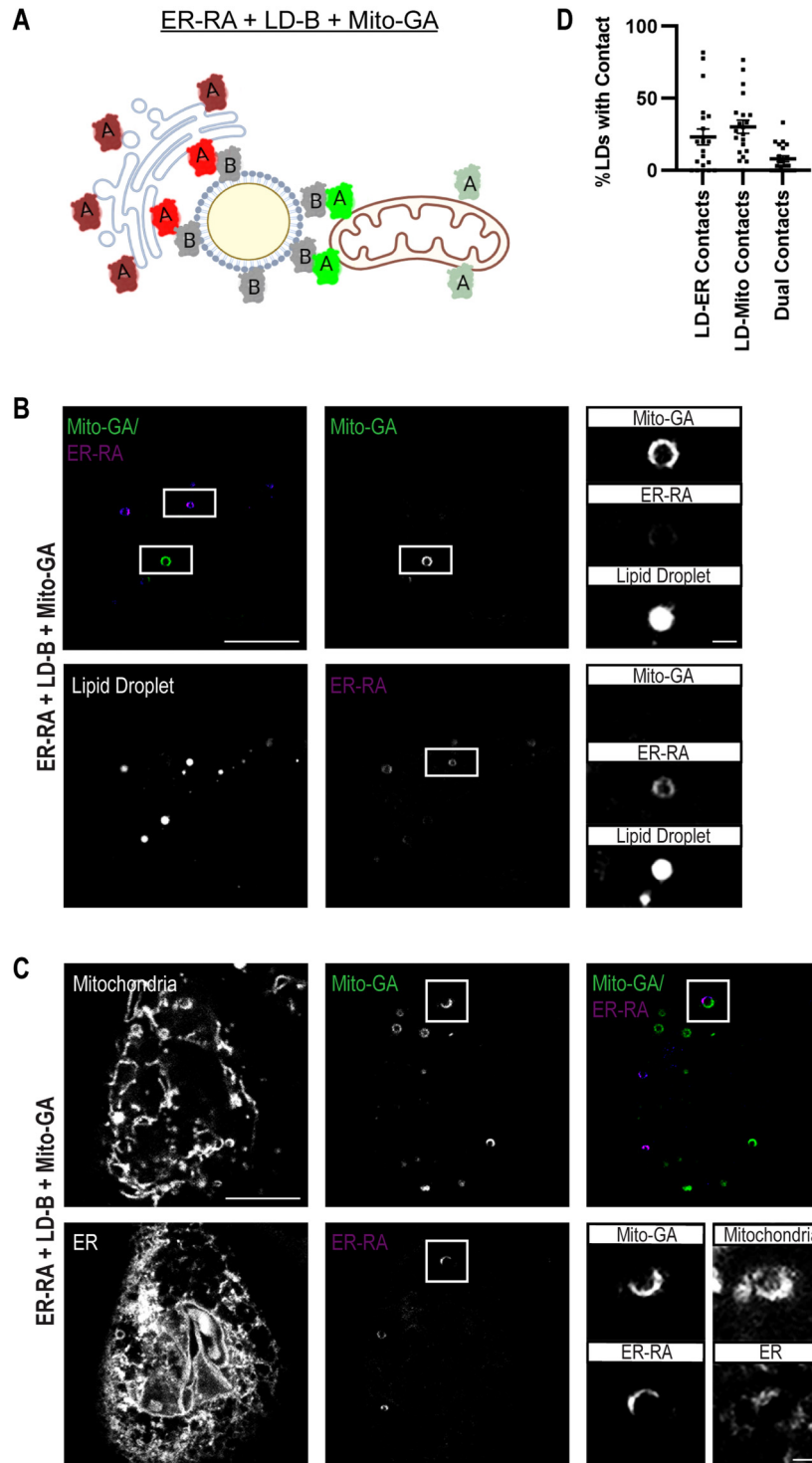


Figure 6. Use case for Contact-FP probes: visualizing multiple MCSs. (A) Cartoon depicting the use of Contact-FP probes (Mito-GA, ER-RA, and LD-B) to simultaneously visualize LD-mitochondria and LD-ER MCSs. Cartoon created with Biorender.com. (B) Single focal plane micrographs of U-2 OS cells transfected with the indicated constructs and labeled for LDs with Lipi-blue. The merged micrograph includes GA and RA channels to demonstrate mitochondria and ER MCSs are spatially distinct. (C) Single focal plane micrographs of U-2 OS cells transfected with the indicated constructs, labeled for mitochondria with MitoTracker Deep Red and labeled for ER with TagBFP-KDEL. The merged micrograph includes GA and RA channels to demonstrate Mito and ER MCSs are spatially distinct. (D) Quantification of images from (B). Twenty-one cells were analyzed across $N=3$ biological replicates. Scale bar, 10 μm . Inset scale bar, 1 μm . Error bars represent \pm SEM. Note. Contact-FP = contact-fluorescent protein; MCS = membrane contact site; Mito-GA = mitochondria-targeted green A; ER = endoplasmic reticulum; RA = red A; LD = lipid droplet; LD-B = LD-tethered B monomer; GA = green A; SEM = standard error of the mean.

We envision that Contact-FP will prove useful for characterizing MCSs in many contexts. It will be fascinating to catalog the abundance and dynamics of MCSs in different cell types, which can have highly specialized organelle morphologies and dynamics. MCSs can remodel in response to developmental or environmental cues (Prinz et al., 2019; Bohnert, 2020). We anticipate that Contact-FP will provide insight into how MCS dynamics change throughout processes such as cell division, migration, and differentiation. Because Contact-FP works on short timescales, it will also be useful for measuring changes in MCS dynamics in response to acute changes such as infection, nutritional fluctuations, and pharmacological perturbations. Finally, it may eventually be possible to introduce Contact-FP probes *in vivo*, allowing minimally perturbing characterization of MCSs in the context of developing and aging organisms, and in various models of human diseases.

Resource Availability

Lead Contact

Further information and requests about resources and reagents are available from the corresponding author, upon reasonable request.

Materials Availability

Plasmids generated in this study are available on Addgene, or from the lead contact on request.

Data Availability

Any additional information required to reanalyze the data reported in this paper is available from the lead contact upon reasonable request.

Experimental Model and Subject Details

U-2 OS cells were obtained from the UNC Tissue Culture Facility and maintained in Dulbecco's Modified Eagle Medium with 10% fetal bovine serum and 4 mM glutamine (complete medium). Cells were cultured on chambered cover glass (#1.5 high-performance cover glass, Cellvis), coated with 10 $\mu\text{g}/\text{mL}$ fibronectin (MilliporeSigma).

Method Details

Cell Transfection

Cells were transfected with mApple-TOMM20-N-10, mApple-Lysosomes-20, mApple-Sec61B, mApple-Peroxisomes-2, mApple-Farnesyl-5, mApple-Caveolin-C-10, TagBFP-KDEL, or Contact-FP constructs using Lipofectamine 2000 (Invitrogen), according to the manufacturer's instructions. All experiments

were performed in eight-well chambered cover glass (Cellvis). Cells were transfected with the following range of plasmid amounts: Cyto-B/Cyto-GA (200–50 ng), LD-B (50–10 ng) and Organelle-GA (100–10 ng). Cells were imaged either 24 h following transfection, or 48 h following transfection if LD-B was used.

Plasmids

Contact-FP constructs were generated using the HiFi DNA Assembly Master mix (New England Biolabs, E2621). For plasmid construction, all polymerase chain reactions were performed using Q5 High Fidelity DNA polymerase (M0419; New England Biolabs) and restriction enzymes from New England Biolabs. The following plasmids were kind gifts: RA-NES, GA-NES, and GB-NES from Robert Campbell (University of Alberta; Ding et al., 2015), TagBFP-KDEL, RA-Sec61B, GA-MFF, and GB-Dcp1b from Gia Voeltz (University of Colorado; Friedman et al., 2011; Lee et al., 2020), Apex2-OMM and ERM-Apex2 from Alice Ting (Stanford; Lam et al., 2014), PM-FRB-CFP from Tamas Balla (NICHHD; Varnai et al., 2006), Lamp1-mTurquoise2 from Dorus Gadella (University of Amsterdam; Chertkova et al., 2020, BioRxiv, 160374), cavin-1-mEGFP from Ari Helenius (ETH Zurich; Hayer et al., 2010), mApple-TOMM20-N-10, mApple-Lysosomes-20, mApple-Peroxisomes-2, mApple-Farnesyl-5, and mApple-Caveolin-C-10 from Michael Davidson (Florida State University), and mEmerald-GPAT4(152-208) and mApple-Sec61B from Jennifer Lippincott-Schwartz (Janelia Research Campus; Nixon-Abell et al., 2016; Chang et al., 2019).

Chemicals and Dyes

The following chemicals and dyes were used: 10 $\mu\text{g}/\text{mL}$ fibronectin (MilliporeSigma), 50 ng/mL Bodipy 665/676 (Life Technologies), 100 nM MitoTracker Deep Red (Life Technologies), 50 nM Lipi-Blue (Dojindo).

Microscopy and Image Processing

Images were acquired on an inverted Zeiss 800/Airyscan laser scanning confocal microscope equipped with 405, 488, 561, and 647 nm diode lasers, and Galium Arsenide Phosphide (GaAsP) and Airyscan detectors. Confocal and Airyscan images were acquired using a 63 \times /1.4 numerical aperture objective lens, at 37 °C and 5% CO₂ (Carl Zeiss, Oberkochen, Germany). Airyscan images were processed in Zen software (Carl Zeiss) using a processing strength of 6.0. Image brightness and contrast were adjusted in Adobe Photoshop CS.

Quantification and Statistical Analysis

Images were analyzed using CellProfiler (Stirling et al., 2021). For colocalization, masks of LD, mitochondria, and GA were created using the corresponding channels. For the

overlap of LDs with mitochondria and GA, the percentage of LD pixels colocalized with the mitochondria or GA versus total LD pixels was calculated. Statistical details for all experiments can be found in the figure legends. Statistical analysis among groups was performed using Student's *t* test.




Declaration of Conflicting Interests

The authors declared no potential conflicts of interest with respect to the research, authorship, and/or publication of this article.

Funding

The authors disclosed receipt of the following financial support for the research, authorship, and/or publication of this article: This work was supported by the National Science Foundation, National Institute of General Medical Sciences, (grant numbers 2010124, R25GM089569, R35GM133460, and T32GM133364).

ORCID iDs

Gregory E. Miner  <https://orcid.org/0000-0002-1124-4217>
 Maria Clara Zanellati  <https://orcid.org/0000-0003-0597-4923>
 Sarah Cohen  <https://orcid.org/0000-0003-2982-3265>

Supplemental Material

Supplemental material for this article is available online.

References

- Abrisch RG, Gumbin SC, Wisniewski BT, Lackner LL, Voeltz GK (2020). Fission and fusion machineries converge at ER contact sites to regulate mitochondrial morphology. *J Cell Biol* 219, e201911122. doi: 10.1083/JCB.201911122/VIDEO-9
- Alford SC, Abdelfattah AS, Ding Y, Campbell RE (2012a). A fluorogenic red fluorescent protein heterodimer. *Chem Biol* 19, 353–360. doi: 10.1016/J.CHEMBIOL.2012.01.006
- Alford SC, Ding Y, Simmen T, Campbell RE (2012b). Dimerization-dependent green and yellow fluorescent proteins. *ACS Synth Biol* 1, 569–575. doi: 10.1021/SB300050J
- Bohnert M (2020). Tether me, tether me not—dynamic organelle contact sites in metabolic rewiring. *Dev Cell* 54, 212–225. doi: 10.1016/J.DEVCEL.2020.06.026
- Castro IG, Shortill SP, Dziurdzik SK, Cadou A, Ganesan S, Valenti R, David Y, Davey M, Mattes C, Thomas FB, et al. (2022). Systematic analysis of membrane contact sites in *Saccharomyces cerevisiae* uncovers modulators of cellular lipid distribution. *ELife* 11, e74602. doi: 10.7554/ELIFE.74602
- Chang CL, Weigel AV, Ioannou MS, Amalia Pasolli H, Shan Xu C, Peale DR, Shtengel G, Freeman M, Hess HF, Blackstone C, Lippincott-Schwartz J (2019). Spastin tethers lipid droplets to peroxisomes and directs fatty acid trafficking through ESCRT-III. *J Cell Biol* 218, 2583. doi: 10.1083/JCB.201902061
- Chertkova AO, Mastop M, Postma M, van Bommel N, van der Niet S, Batenburg KL, Joosen L, Gadella TWJ, Okada Y, Goedhart J (2020). Robust and bright genetically encoded fluorescent markers for highlighting structures and compartments in mammalian cells. *BioRxiv* 160374. doi: 10.1101/160374
- Cho KF, Branon TC, Rajeev S, Svinkina T, Udeshi ND, Thoudam T, Kwak C, Rhee HW, Lee IK, Carr SA, Ting AY (2020). Split-TurboID enables contact-dependent proximity labeling in cells. *Proc Natl Acad Sci USA* 117, 12143. doi: 10.1073/PNAS.1919528117/-DCSUPPLEMENTAL
- Chung J, Wu X, Lambert TJ, Lai ZW, Walther TC, Farese RV (2019). Lipid droplet assembly factor-1 and seipin form a lipid droplet assembly complex. *Dev Cell* 51, 551. doi: 10.1016/J.DEVCEL.2019.10.006
- Cieri D, Vicario M, Giacomello M, Vallese F, Filadi R, Wagner T, Pozzan T, Pizzo P, Scorrano L, Brini M, Cali T (2017). SPLICS: A split green fluorescent protein-based contact site sensor for narrow and wide heterotypic organelle juxtaposition. *Cell Death Diff* 25, 1131–1145. doi: 10.1038/s41418-017-0033-z
- Ding Y, Li J, Enterina JR, Shen Y, Zhang I, Tewson PH, Mo GCH, Zhang J, Quinn AM, Hughes TE, et al. (2015). Ratiometric biosensors based on dimerization-dependent fluorescent protein exchange. *Nat Methods* 12, 195–198. doi: 10.1038/nmeth.3261
- Friedman JR, Lackner LL, West M, DiBenedetto JR, Nunnari J, Voeltz GK (2011). ER Tubules mark sites of mitochondrial division. *Science* 334, 358–362. doi: 10.1126/SCIENCE.1207385/SUPPL_FILE/FRIEDMAN.SOM.REV1.PDF
- Hayer A, Stoeber M, Bissig C, Helenius A (2010). Biogenesis of caveolae: Stepwise assembly of large caveolin and cavin complexes. *Traffic* 11, 361–382. doi: 10.1111/J.1600-0854.2009.01023.X
- Jing J, Liu G, Huang Y, Zhou Y (2020). A molecular toolbox for interrogation of membrane contact sites. *J Physiol* 598, 1725. doi: 10.1113/JP277761
- Kakimoto Y, Tashiro S, Kojima R, Morozumi Y, Endo T, Tamura Y (2018). Visualizing multiple inter-organelle contact sites using the organelle-targeted split-GFP system. *Sci Rep* 8, 1–13. doi: 10.1038/s41598-018-24466-0
- Kwak C, Shin S, Park JS, Jung M, My Nhung TT, Kang MG, Lee C, Kwon TH, Park SK, Mun JY, Kim JS, Rhee HW (2020). Contact-ID, a tool for profiling organelle contact sites, reveals regulatory proteins of mitochondrial-associated membrane formation. *Proc Natl Acad Sci USA* 117, 12109–12120. doi: 10.1073/pnas.1916584117
- Lahiri S, Chao JT, Tavassoli S, Wong AKO, Choudhary V, Young BP, Loewen CJR, Prinz WA (2014). A conserved endoplasmic reticulum membrane protein complex (EMC) facilitates phospholipid transfer from the ER to mitochondria. *PLOS Bio* 12, e1001969. doi: 10.1371/JOURNAL.PBIO.1001969
- Lam SS, Martell JD, Kamer KJ, Deerinck TJ, Ellisman MH, Mootha VK, Ting AY (2014). Directed evolution of APEX2 for electron microscopy and proximity labeling. *Nat Methods* 12, 51–54. doi: 10.1038/nmeth.3179
- Lee JE, Cathey PI, Wu H, Parker R, Voeltz GK (2020). Endoplasmic reticulum contact sites regulate the dynamics of membraneless organelles. *Science* 367, eaay7108. doi: 10.1126/SCIENCE.AAY7108/SUPPL_FILE/AAY7108_LEE_SM.PDF
- Matthaeus C, Taraska JW (2021). Energy and dynamics of caveolae trafficking. *Front Cell Dev Biol* 8, 614472. doi: 10.3389/FCCELL.2020.614472/BIBTEX
- Miner GE, So CM, Edwards W, Ragusa JV, Wine JT, Wong Gutierrez D, Airola MV, Herring LE, Coleman RA, Klett EL, Cohen S (2023). PLIN5 Interacts with FATP4 at membrane contact sites to promote lipid droplet-to-mitochondria fatty acid transport. *Dev Cell* 58, 1250–1265.e6. doi: 10.1016/J.DEVCEL.2023.05.006
- Naon D, Zaninello M, Giacomello M, Varanita T, Grespi F, Lakshminaranayan S, Serafini A, Semenzato M, Herkenne S,

- Hernández-Alvarez MI, et al. (2016). Critical reappraisal confirms that mitofusin 2 is an endoplasmic reticulum-mitochondria tether. *Proc Natl Acad Sci USA* *113*, 11249–11254. doi: 10.1073/PNAS.1606786113/SUPPL_FILE/PNAS.201606786SI.PDF
- Nguyen TT, Voeltz GK (2022). An ER phospholipid hydrolase drives ER-associated mitochondrial constriction for fission and fusion. *ELife* *11*, e84279. doi: 10.7554/ELIFE.84279
- Nixon-Abell J, Obara CJ, Weigel AV, Li D, Legant WR, Xu CS, Pasolli HA, Harvey K, Hess HF, Betzig E, et al. (2016). Increased spatiotemporal resolution reveals highly dynamic dense tubular matrices in the peripheral ER. *Science* *354*(6311), aaf3928. doi: 10.1126/SCIENCE.AAF3928/SUPPL_FILE/NIXON-ABELL.SM.PDF
- Prinz WA, Toulmay A, Balla T (2019). The functional universe of membrane contact sites. *Nat Rev Mol Cell Biol* *21*, 7–24. doi: 10.1038/s41580-019-0180-9
- Scorrano L, De Matteis MA, Emr S, Giordano F, Hajnóczky G, Kornmann B, Lackner LL, Levine TP, Pellegrini L, Reinisch K, et al. (2019). Coming together to define membrane contact sites. *Nat Commun* *10*, 1–11. doi: 10.1038/s41467-019-09253-3
- Shai N, Yifrach E, Van Roermund CWT, Cohen N, Bibi C, Ijlst L, Cavellini L, Meurisse J, Schuster R, Zada L, et al. (2018). Systematic mapping of contact sites reveals tethers and a function for the peroxisome-mitochondria contact. *Nat Commun* *9*, 1–13. doi: 10.1038/s41467-018-03957-8
- Soukupova M, Sprenger C, Gorgas K, Kunau WH, Dodt G (1999). Identification and characterization of the human peroxin PEX3. *Euro J Cell Biol* *78*, 357–374. doi: 10.1016/S0171-9335(99)80078-8
- Stirling DR, Swain-Bowden MJ, Lucas AM, Carpenter AE, Cimini BA, Goodman A (2021). Cellprofiler 4: Improvements in speed, utility and usability. *BMC Bioinform* *22*, 1–11. doi: 10.1186/S12859-021-04344-9/FIGURES/6
- Vallese F, Catoni C, Cieri D, Barazzuol L, Ramirez O, Calore V, Bonora M, Giamogante F, Pinton P, Brini M, Cali T (2020). An expanded palette of improved SPLICS reporters detects multiple organelle contacts in vitro and in vivo. *Nat Commun* *11*, 1–15. doi: 10.1038/s41467-020-19892-6
- Valm AM, Cohen S, Legant WR, Melunis J, Hershberg U, Wait E, Cohen AR, Davidson MW, Betzig E, Lippincott-Schwartz J (2017). Applying systems-level spectral imaging and analysis to reveal the organelle interactome. *Nature* *546*, 162–167. doi: 10.1038/nature22369
- Varnai P, Thyagarajan B, Rohacs T, Balla T (2006). Rapidly inducible changes in phosphatidylinositol 4,5-bisphosphate levels influence multiple regulatory functions of the lipid in intact living cells. *J Cell Biol* *175*, 377–382. doi: 10.1083/JCB.200607116
- Wang H, Becuwe M, Housden BE, Chitraju C, Porras AJ, Graham MM, Liu XN, Thiam AR, Savage DB, Agarwal AK, et al. (2016). Seipin is required for converting nascent to mature lipid droplets. *ELife* *5*(AUGUST), e16582. doi: 10.7554/ELIFE.16582
- Wang H, Sreenivasan U, Hu H, Saladino A, Polster BM, Lund LM, Gong D, Stanley WC, Sztalryd C (2011). Perilipin 5, a lipid droplet-associated protein, provides physical and metabolic linkage to mitochondria. *J Lipid Res* *52*, 2159. doi: 10.1194/JLR.M017939
- Wilfling F, Wang H, Haas JT, Kraemer N, Gould TJ, Uchida A, Cheng J-X, Graham M, Christiano R, Fröhlich F, et al. (2013). Triacylglycerol synthesis enzymes mediate lipid droplet growth by relocalizing from the ER to lipid droplets. *Dev Cell* *24*, 384–399. doi: 10.1016/j.devcel.2013.01.013
- Yang Z, Zhao X, Xu J, Shang W, Tong C (2018). A novel fluorescent reporter detects plastic remodeling of mitochondria-ER contact sites. *J Cell Sci* *131*, jcs208686. doi: 10.1242/JCS.208686/VIDEO-1